brian fossils (*20*) have led to the reinterpretation of the affinities of other apparently bizarre forms, removing them from the problematica. The recognition of taxa as problematic is a statement of ignorance—an artifact of our level of knowledge and imperfect resolution of relationships. These new discoveries, like the analysis presented here, have damped the Cambrian "explosion." Whereas a morphospace equivalent to that occupied by the range of modern arthropods was filled relatively rapidly, the evidence provides little justification for invoking special evolutionary processes to explain the early radiation of the metazoans.

REFERENCES AND NOTES

1. S. Conway Morris, *Science* **246**, 339 (1989); *Trans. R. Soc. Edinb. Earth Sci.* **80**, 271 (1989).
2. H. B. Whittington, *Proc. Geol. Assoc.* **91**, 127 (1980); *Proc. Linn. Soc. N.S.W.* **105**, 79 (1981); in *Palaeontology: Essential of Historical Geology*, E. M. Gallitelli, Ed. (Mucchi, Modena, Italy, 1982), pp. 11–24; D. E. G. Briggs and S. Conway Morris, in *Problematic Fossil Taxa*, A. Hoffman and M. H. Nitecki, Eds. (Oxford Univ. Press, New York, 1986), pp. 167–183.
3. S. J. Gould, *Wonderful Life: The Burgess Shale and the Nature of History* (Norton, New York, 1989).
4. B. Runnegar, in *Rates of Evolution*, K. S. W. Campbell and M. F. Day, Eds. (Allen & Unwin, London, 1987), pp. 39–60.
5. J. W. Valentine and D. H. Erwin, in *Development as an Evolutionary Process*, R. A. Raff and E. C. Raff, Eds. (Liss, New York, 1987), pp. 71–107.
6. S. Conway Morris, *Palaeontology (London)* **29**, 423 (1986).
7. H. B. Whittington, *The Burgess Shale* (Yale Univ. Press, New Haven, CT, 1985), pp. 1–151.
8. D'A. W. Thompson, *On Growth and Form* (Cambridge Univ. Press, Cambridge, 1961).
9. M. Foote, *Syst. Zool.* **39**, 371 (1990); *Palaeontology (London)* **34**, 461 (1991).
10. _____, *Univ. Mich. Mus. Paleontol. Contribs.* **28**, 101 (1991).
11. F. L. Bookstein *et al.*, *Acad. Nat. Sci. Philadelphia Spec. Pub.* **15**, 1 (1985).
12. D. E. G. Briggs and H. B. Whittington, *Trans. R. Soc. Edinburgh Earth Sci.* **76**, 149 (1985).
13. The data matrix used in both the phenetic and cladistic analyses can be obtained from the authors.
14. D. E. G. Briggs and H. B. Whittington, *U.S. Geol. Surv. Open-File Rep. 81-743* (1981), pp. 38–41.
15. S. J. Gould, *Paleobiology* **17**, 411 (1991).
16. D. E. G. Briggs and R. A. Fortey, in *Origins and Early Evolutionary History of the Metazoa*, J. W. Lipps and P. W. Signor, Eds. (Plenum, New York, 1992), pp. 335–373.
17. D. E. G. Briggs, in *Arthropod Paleobiology* (*Short Courses in Paleontology* (Paleontological Society, University of Tennessee, Knoxville, 1990) vol. 3, pp. 24–43.
18. _____, in *Crustacean Phylogeny*, F. R. Schram, Ed. (Balkema, Rotterdam, 1979), pp. 1–22.
19. _____ and R. A. Fortey, *Science* **246**, 241 (1989).
20. S. Conway Morris and J. S. Peel, *Nature* **345**, 802 (1990); L. Ramsköld and H. Xianguang, *ibid.* **351**, 225 (1991).

21. We acknowledge, with thanks, comments and discussion on the quantification of disparity and on phylogenetic analysis from G. A. Boxshall, S. Conway Morris, A. Dennis, S. J. Gould, W. L. Kovach, M. Foote, P. L. Forey, C. Moncrieff, J. M. V. Rayner, J. J. Sepkoski, P. H. A. Sneath, A. Swan, J. T. Temple, and M. Wilkinson. J. W. Archie generously supplied software. M.A.W. was funded by a University of Bristol postgraduate scholarship.

4 February 1992; accepted 29 April 1992

Three-Dimensional Solution Structure of Human Interleukin-4 by Multidimensional Heteronuclear Magnetic Resonance Spectroscopy

Robert Powers, Daniel S. Garrett, Carl J. March, Eric A. Frieden, Angela M. Gronenborn,* G. Marius Clore*

The three-dimensional solution structure of recombinant human interleukin-4, a protein of 133 residues and 15.4 kilodaltons that plays a key role in the immune and inflammatory systems, has been solved by multidimensional heteronuclear magnetic resonance spectroscopy. The structure is dominated by a left-handed four-helix bundle with an unusual topology comprising two overhand connections. The linker elements between the helices are formed by either long loops, small helical turns, or short strands. The overall topology is remarkably similar to that of growth hormone and granulocyte-macrophage colony stimulating factor, despite the absence of any sequence homology, and substantial differences in the relative lengths of the helices, the length and nature of the various connecting elements, and the pattern of disulfide bridges. These three proteins, however, bind to cell surface receptors belonging to the same hematopoietic superfamily, which suggests that interleukin-4 may interact with its receptor in an analogous manner to that observed in the crystal structure of the growth hormone-extracellular receptor complex.

Interleukin-4 (IL-4) is one of a group of cytokines that play a central role in the control and regulation of the immune and inflammatory systems (*1*). Specific activities associated with IL-4 are the stimulation of activated B cell, T lymphocyte, thymocyte, and mast cell proliferation and the induction of cytotoxic $CD8^+$ T cells. The latter is responsible for the antitumor activity of IL-4. Renal tumor cells that secrete large doses of IL-4 can establish tumor-specific immunity toward a preexisting renal cancer (*2*). In addition, IL-4 induces the expression of class II major histocompatibility complex (MHC) molecules and the immunoglobulin E (IgE) low-affinity receptor on resting B cells (*3*). Further, IL-4 is responsible for generating and sustaining in vivo IgE responses and for ensuring the dominance of IgG1 in the T cell–dependent immune response by causing immunoglobulin class switching of activated B cells to IgE and IgG1, respectively (*3*). In order to provide a structural basis for understanding the mode of action of IL-4 and its interaction with its cell surface receptor, we have determined the three-dimensional (3D) structure of human recombinant IL-4 (15.4 kD and 133 residues) in solution using multidimensional heteronuclear NMR (nuclear magnetic resonance) spectroscopy.

The NMR structure determination was principally based on 823 approximate interproton distance restraints derived from 3D ^{15}N- (*4*) and ^{13}C-separated (*5*) NOESY (nuclear Overhauser enhancement spectroscopy) spectra and a ^1H-^{15}N HMQC (heteronuclear multiple quantum coherence)–NOESY-HMQC spectrum (*6*) recorded on uniformly (>95%) labeled ^{15}N- and ^{13}C-^{15}N–labeled human recombinant IL-4 (*7*, *8*). These spectra were interpreted on the basis of complete ^1H, ^{15}N, and ^{13}C assignments obtained previously with 3D double- and triple-resonance NMR spectroscopy (*9*). [Note that a partial set of ^1H and ^{15}N assignments has also been published by Redfield *et al.* (*10*)]. An example of the quality of the 3D ^{13}C-separated NOESY spectrum is shown in Fig. 1. The interproton distance restraints were classified into three distance ranges, 1.8 to 2.7 Å, 1.8 to 3.3 Å [1.8 to 3.5 Å for nuclear Overhauser effects (NOEs) involving NH protons], and 1.8 to 5.0 Å, corresponding to strong, medium, and weak NOEs, respectively (*11*, *12*). With the exception of sequential $C\beta H(i)$-$NH(i+1)$ NOEs, all NOEs involving side chains were derived from the 3D ^{13}C-separated NOESY spectrum. Although the ^1H chemical shift dispersion of IL-4 is small (*10*), the increased resolution afforded by separating the NOEs into a third dimension according to the ^{13}C chemical shift of the carbon atom attached to the destination proton is sufficient to extract a large number of NOEs unambiguously by making use of the symmetry relations inherent to this spectrum. Thus, the NOE from proton i to proton j is labeled by the ^{13}C chemical shift of the carbon atom attached to proton j, and the symmetry-related NOE from proton j to proton i is labeled by the ^{13}C chemical shift of the carbon atom attached to proton i. In this

R. Powers, D. S. Garrett, A. M. Gronenborn, G. M. Clore, Laboratory of Chemical Physics, National Institute of Diabetes and Digestive and Kidney Diseases, National Institutes of Health, Bethesda, MD 20892.
C. J. March and E. A. Frieden, Immunex Corporation, 51 University Street, Seattle, Washington 98101.

*To whom correspondence should be addressed.

manner, we readily assigned a large number of interresidue side chain–backbone and side chain–side chain NOE interactions that comprised 188 and 205 restraints, respectively (Fig. 2). The interproton distance restraints were supplemented by 101 ϕ torsion angle restraints derived from $^3J_{HN\alpha}$ coupling constants (*13*), 82 ψ torsion angle restraints within clearly defined helical regions derived from $^{13}C\alpha$ and $^{13}C\beta$ chemical shifts (*14*), and, subsequent to preliminary structure calculations, 98 distance restraints for 49 backbone NH–CO hydrogen bonds derived from slowly exchanging backbone amide resonances (*15*) and the pattern of medium-range ($1 < |i - j| \leq 5$) and interstrand backbone-backbone NOEs within the helical and β-sheet regions, respectively (*16*). There are a total of 1104 experimental NMR restraints. At present no stereospecific assignments of β-methylene protons and methyl groups of Leu and Val have been obtained. Also, the structure calculations do not include any χ_1 torsion angle restraints. Hence the present structure should be regarded as a good-quality second-generation structure (*17*).

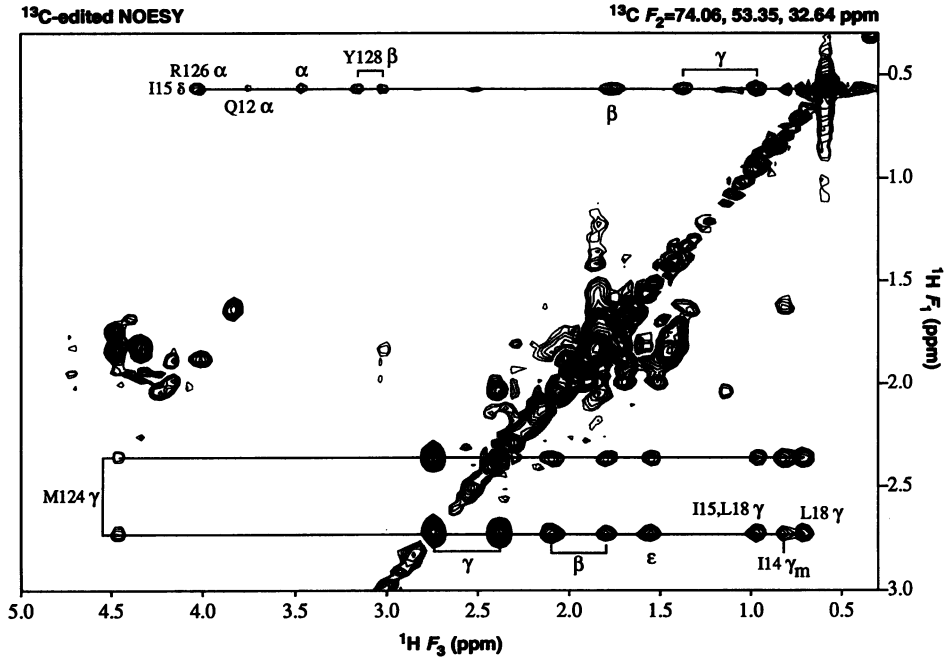

Fig. 1. Example of a $^1H(F_1)$-$^1H(F_3)$ plane taken at $^{13}C(F_2)$ = 53.35 ± 20.71 *n* ppm (where *n* is an integer) of the 100-ms mixing time 3D ^{13}C-separated NOESY spectrum of uniformly (>95%) ^{15}N-^{13}C labeled recombinant human IL-4. A number of long-range NOEs to the $C\delta H_3$ methyl group of Ile^{15} and $C\gamma H$ protons of Met^{124} are indicated. Positive and negative contours (arising as a result of the extensive folding used in the ^{13}C dimension) are indicated by solid and dashed lines, respectively.

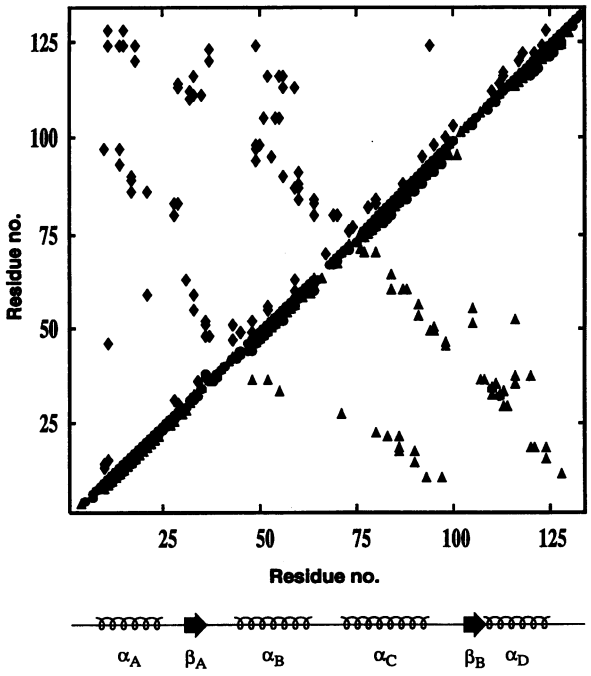

Fig. 2. Summary of the NOE connectivities assigned in the 3D heteronuclear spectra of recombinant human IL-4. Side chain–side chain NOEs (◆) are shown above the diagonal and side-chain–backbone (▲) and backbone-backbone (●) NOEs are below the diagonal. The location of the four long helices comprising the four-helix bundle and the two strands is indicated below the figure.

A total of 22 simulated annealing (SA) structures (*18*) were calculated with the hybrid-distance geometry–simulated annealing protocol of Nilges *et al.* (*19, 20*) (Table 1). All of the structures satisfy the NMR restraints within experimental error (that is, no violations greater than 0.5 Å and 5° for the distance and torsion angle restraints, respectively), exhibit very small deviations from idealized covalent geometry, and display good nonbonded contacts as judged by the large negative values of the calculated Lennard-Jones van der Waals energy (*21*) and the solvation free energy of folding (*22*). A best-fit superposition of the 22 SA structures is shown in Fig. 3A. Residues 1 to 6, 132, and 133 are disordered; only residues 6 to 132 are shown in Fig. 3. The atomic root-mean-square (rms) distribution about the mean coordinate positions for residues 7 to 131 is 1.02 ± 0.16 Å for the backbone atoms and 1.50 ± 0.17 Å for all atoms; the corresponding rms values for the regions of secondary structure (residues 7 to 24, 26 to 36, 45 to 64, 67 to 70, 74 to 96, and 107 to 129) are 0.79 ± 0.13 and 1.25 ± 0.27 Å, respectively (*23*).

The IL-4 molecule is oblong in shape with approximate dimensions of 41 Å by 28 Å by 19 Å. The major topological feature is a left-handed four-helix bundle with an unusual connectivity in which helices adjacent to each other on a square lattice are antiparallel, whereas nonadjacent opposing helices are parallel. Thus the bundle has two overhand connections (Fig. 4). The angles and axial separations between the long axes of the four antiparallel helical pairs, α_A-α_C, α_C-α_B, α_B-α_D, and α_D-α_A, are −153° and 9.0 Å, −148° and 5.9 Å, −142° and 10.3 Å, and −154° and 9.1 Å, respectively. The corresponding values between the two parallel helical pairs, α_A-α_B and α_C-α_D, are 42° and 11.9 Å and 45° and 13.8 Å, respectively. The four helices have approximately similar lengths and comprise residues 7 to 24 (α_A), 45 to 64 (α_B), 74 to 96 (α_C), and 113 to 129 (α_D). The connecting elements between the helices are formed by either long loops, small helical turns, or short strands. Specifically, helix α_A leads into a five-residue helical turn (ht_A, residues 26 to 30) followed by a strand (β_A, residues 31 to 36) that runs in an antiparallel direction to helix α_A and a loop (residues 37 to 44) that leads into helix α_B. Helices α_B and α_C are connected by a short loop (residues 65 to 73) that contains a short four-residue helical turn (ht_B, residues 67 to 70). The two

helical turns, ht_A and ht_B, are connected to each other by a disulfide bridge between Cys^{28} and Cys^{69}. Helix α_C leads into a loop (residues 97 to 106) and a short strand (β_B, residues 107 to 112) that runs antiparallel to α_C and leads directly into the fourth helix α_D. The loop from residues 97 to 106 is connected to helix α_B through a disulfide bridge between Cys^{103} and Cys^{50}. The two strands form a mini-antiparallel β sheet comprising residues 32 to 34 of β_A and 110 to 112 of β_B. Finally, the amino terminus of helix α_A and the carboxyl-terminal end of IL-4 are connected by the disulfide bridge between Cys^7 and Cys^{131}.

The internal core of the four-helix bundle is entirely hydrophobic in nature and consists of Leu^{11}, Ile^{14}, Leu^{18}, and Leu^{21} of α_A, Phe^{49}, Ala^{52}, Leu^{56}, Phe^{59}, and Tyr^{60} of α_B, Ile^{84}, Leu^{87}, Leu^{90}, Leu^{94}, and Leu^{97} of α_C, and Leu^{113}, Leu^{117}, Leu^{120}, Met^{124}, and Tyr^{128} of α_D. The packing within the hydrophobic core is shown in Fig. 3B. In addition, there are also a number of hydrophobic interactions between β_A (Thr^{34} and Ile^{36}) and α_B (Val^{55} and Ala^{52}), β_A (Val^{33}, Ile^{36}, and Phe^{37}) and α_D (Leu^{113}, Phe^{116}, Leu^{120}, and Ile^{123}), and β_A (Thr^{34}) and β_B (Ala^{108}) (Fig. 3B). Turns ht_A and ht_B are in part stabilized by side chain–backbone hydrogen bonds such as the one between Thr^{29} OγH and the backbone CO of Lys^{25}, and the one between the side chain carboxylate of Asp^{66} and the backbone NH of Cys^{69}, respectively. The exterior of IL-4, on the other hand, is hydrophilic and contains a large number of positively charged Lys and Arg residues.

To our knowledge, the topology of the left-handed four-helix bundle seen in IL-4 has only been observed twice previously, namely, in the cases of growth hormone (*24*, *25*) and granulocyte-macrophage colony-

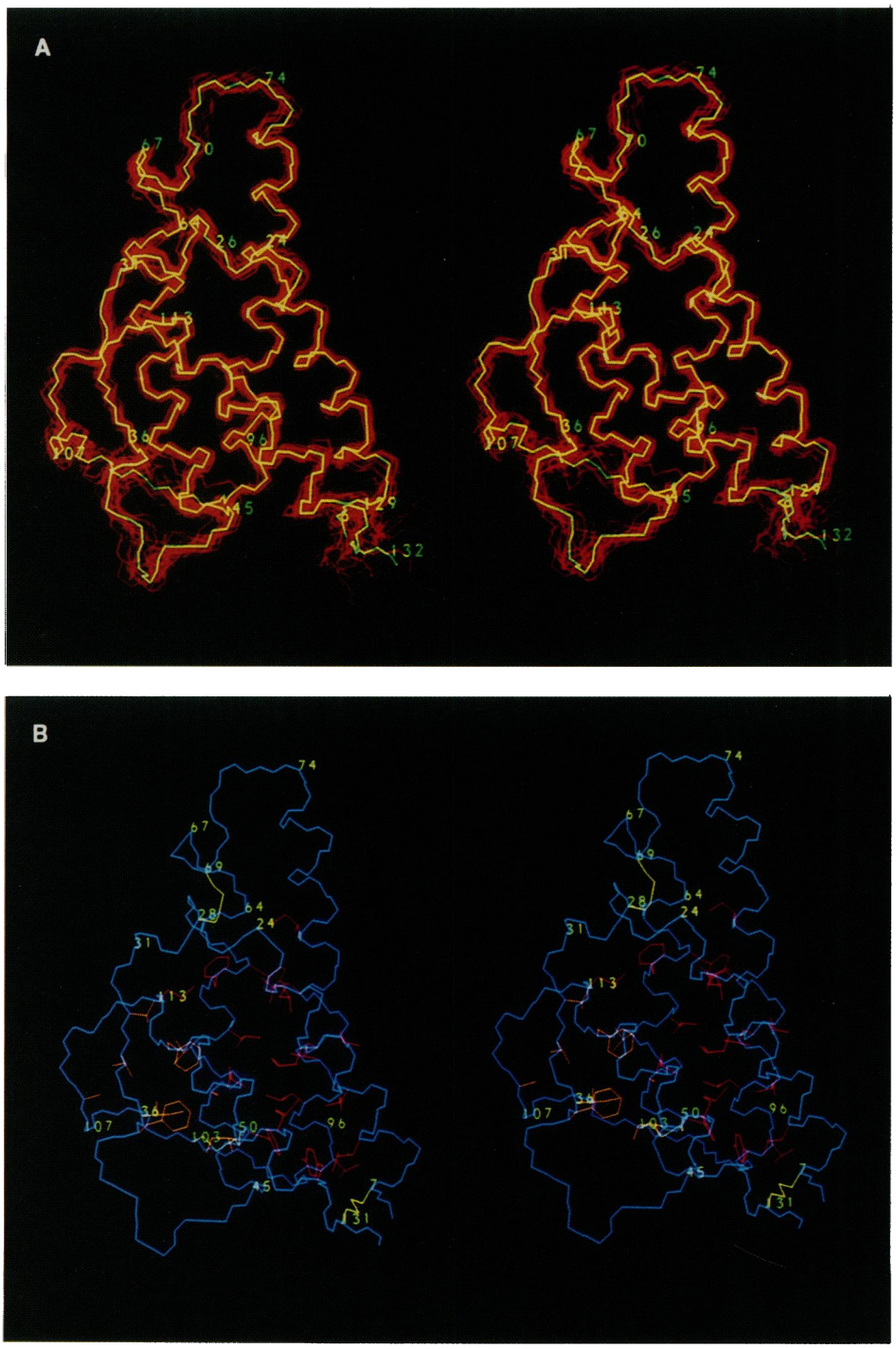

Fig. 3. (**A**) Stereoview of the best-fit superposition of the backbone (N, Cα, and C) atoms of the 22 SA structures (red) of recombinant human IL-4. Only residues 6 to 132 are shown as the amino and carboxyl termini are disordered, and the native sequence starts at residue 5. The restrained minimized mean (SA)r structure is shown in yellow to guide the eye. (**B**) Stereoview of the restrained minimized mean (SA)r structure illustrating the hydrophobic packing within the core of the protein. The backbone is shown in blue, the three disulfide bridges (Cys^7-Cys^{131}, Cys^{28}-Cys^{69}, and Cys^{50}-Cys^{103}) in yellow, the hydrophobic residues within the core of the four-helix bundle in red, and the residues involved in hydrophobic interactions between the two strands and helices α_B and α_D in orange.

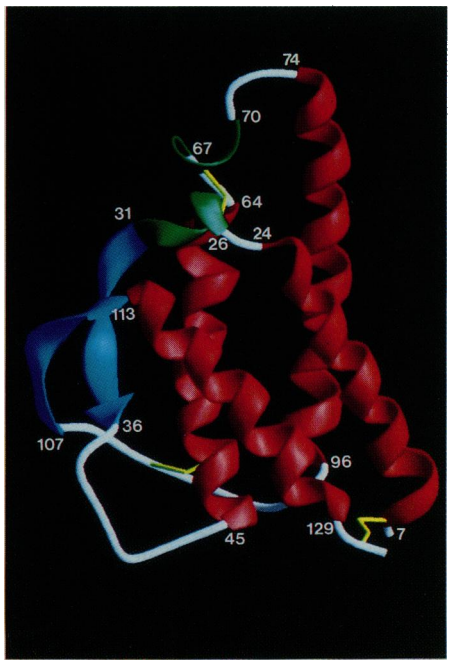

Fig. 4. Ribbon drawing of the restrained minimized mean (SA)r structure of recombinant human IL-4. Residues 6 to 131 are shown. The four helices (α_A, α_B, α_C, and α_D) comprising the left-handed four-helix bundle are shown in red, the two small helical turns (ht_A and ht_B) in green, the two short strands (β_A and β_B) in blue, and the three disulfide bridges in yellow. The model was generated with the program Ribbon 2.0 (*32*).

Table 1. Structural statistics. The notation of the structures is as follows: ⟨SA⟩ are the 22 SA structures; $\overline{SA}$ is the mean structure obtained by averaging the coordinates of the individual SA structures best fitted to each other (the residues used in the best fitting are 7 to 131); and ($\overline{SA}$)r is the restrained minimized (regularized) mean structure obtained from $\overline{SA}$. The number of terms for the various restraints are given in parentheses; rms, root-mean-square; and expt, experimental.

Parameter	⟨SA⟩	($\overline{SA}$)r
Rms deviations from expt distance restraints (Å)*		
All (921)	0.033 ± 0.005	0.031
Sequential ($\|i - j\| = 1$) (283)	0.033 ± 0.004	0.028
Medium range ($1 < \|i - j\| \leq 5$) (305)	0.034 ± 0.007	0.029
Long range ($\|i - j\| > 5$) (235)	0.033 ± 0.010	0.039
Hydrogen-bond restraints (98)†	0.029 ± 0.006	0.023
Rms deviation from expt torsion		
Angle restraints (degrees) (183)‡	0.293 ± 0.088	0.288
Deviations from idealized covalent geometry§		
Bonds (Å) (2175)	0.002 ± 0.0003	0.002
Angles (degrees) (3929)	0.362 ± 0.040	0.327
Impropers (degrees) (835)	0.346 ± 0.053	0.297
E_{L-J} (kcal mol^{-1})‖	−410 ± 10	−396
SFE (kcal/mol^{-1})¶	−139 ± 3	−149

*None of the structures exhibit distance violations greater than 0.5 Å or dihedral-angle violations greater than 5°. No intraresidue interproton distance restraints were used in the calculations. The medium-range NOEs comprise 140 backbone-backbone; 113 side chain–backbone, and 52 side chain–side chain NOEs, and the long-range NOEs comprise 7 backbone-backbone, 75 side chain–backbone, and 153 side chain–side-chain NOEs. †Each hydrogen bond is characterized by two distance restraints: $r_{NH-O} \leq 2.3$ Å and $r_{N-O} = 2.5$ to 3.3 Å. All hydrogen-bonding restraints include slowly exchanging backbone amide protons. ‡There are 101 ϕ and 82 ψ backbone torsion angle restraints (*13, 14*). §The improper torsion restraints serve to maintain planarity and chirality. ‖E_{L-J} is the Lennard-Jones van der Waals energy calculated with the CHARMM (*21*) empirical energy function and is not included in the target function for simulated annealing or restrained minimization. ¶*SFE* is the calculated solvation free energy of folding (*22*) and is not included in the target function for simulated annealing or minimization. The expected value of the *SFE* for a protein the size of human recombinant IL-4 (133 residues) is −135 kcal mol^{-1} (*22*).

stimulating factor (GM-CSF) (*26*). Although the relative orientations of the four helices comprising the bundle are similar for the three proteins, the structural details are quite distinct, both with regard to the relative lengths of the helices and the length and nature of the various connecting elements. Thus, in the case of growth hormone, helices α_A (26 residues) and α_D (30 residues) are substantially longer than helices α_B (21 residues) and α_C (23 residues), whereas in the case of IL-4 the reverse is true with α_A (18 residues) and α_D (17 residues) being shorter than α_B (20 residues) and α_C (23 residues). In GM-CSF, on the other hand, all four helices are significantly shorter and have lengths ranging from 10 residues for α_D to 16 for α_A, with the other two helices comprising 14 residues each. These differences result in a distinct alteration in the surface at the top of the front face of the three proteins in the view shown in Fig. 4. In addition, the pattern as well as the number of disulfide linkages (two in growth hormone and GM-CSF versus three in IL-4) is different. Finally, there is no sequence similarity between the three proteins.

Nevertheless the overall resemblance between the topologies of IL-4, GM-CSF, and growth hormone is striking given the lack of sequence, disulfide bond, and length similarity. On the other hand, the receptors for these three proteins belong to the same hematopoietic superfamily, which also includes the receptors for interleukins-2, -3, -5, -6, and -7, granulocyte colony stimulating factor, erythropoietin, prolactin, leukemia inhibitory factor, and ciliary neutrophic factor (*27*). The interaction of IL-4 with the extracellular domain of its receptor may be similar to that observed in the crystal structure of the growth hormone–extracellular receptor complex (*25*), in which case IL-4 would interact with the extracellular domains of two receptor molecules and the site of interaction with one receptor would involve the surface formed by helices α_A and α_C, while the other interaction site would involve the surface formed by helix α_D, strand β_A, and the loop connecting β_A to helix α_B. The first site is located at the right-hand lower edge of the molecule in the view shown in Fig. 4 and is made up of Lys^6, Glu^{13}, Lys^{16}, Ser^{20}, Gln^{82}, Arg^{85}, Arg^{89}, and Asn^{93}. The second site is located on the left side of the molecule in the view shown in Fig. 4 and comprises Asp^{35}, Asp^{42}, Glu^{45}, Asn^{115}, Arg^{119}, Glu^{126}, and Lys^{127}. Despite the high degree (~44%) of overall sequence identity between human and mouse IL-4 (*28*), only 5 (Glu^{13}, Asp^{42}, Glu^{45}, Arg^{85}, and Arg^{89}) of the 15 residues proposed to interact with the receptor are conserved, and the substitutions involve either charge removal (for example, Lys^6 → Gly, Lys^{16} → Gly, Asp^{35} → Asn, Arg^{119} → Ser, and Glu^{126} → Met) or charge reversal (Ser^{20} → Glu, Glu^{82} → Arg, and Lys^{127} → Asp). In addition, sequence alignments between the human and mouse IL-4 sequences result in a gap in the mouse sequence relative to the human one either at the beginning (*28*) or end of helix α_C (*29*), and therefore probably constitutes the region with the largest conformational differences between the human and mouse protein. This difference may account for the observation that human and mouse IL-4 do not exhibit cross-species activity with regard to either receptor binding or biological function (*30, 31*).

REFERENCES AND NOTES

1. W. E. Paul and J. Ohara, *Annu. Rev. Immunol.* **5**, 429 (1987); T. Yokota *et al.*, *Immunol. Rev.* **103**, 137 (1988); F. D. Finkelman *et al.*, *Annu. Rev. Immunol.* **8**, 303 (1990).
2. P. T. Golumbek *et al.*, *Science* **254**, 713 (1991).
3. R. Kühn, K. Rajewsky, W. Müller, *ibid.*, p. 707.
4. D. Marion *et al.*, *Biochemistry* **28**, 6150 (1989); E. R. P. Zuiderweg and S. W. Fesik, *ibid.*, p. 2387.
5. M. Ikura, L. E. Kay, R. Tschudin, A. Bax, *J. Magn. Reson.* **86**, 204 (1990); E. R. P. Zuiderweg, L. P. McIntosh, F. W. Dahlquist, S. W. Fesik, *ibid.*, p. 210.
6. M. Ikura, A. Bax, G. M. Clore, A. M. Gronenborn, *J. Am. Chem. Soc.* **112**, 9020 (1990).
7. All of the spectra were recorded at 36°C on an AM600 spectrometer equipped with a triple-resonance ^{1}H, ^{15}N, ^{13}C probe. Quadrature detection in the indirectly detected dimensions was obtained with the TPPI-States method [D. Marion, M. Ikura, R. Tschudin, A. Bax, *J. Magn. Reson.* **85**, 393 (1989)]. The 3D ^{15}N- and ^{13}C-separated NOESY spectra were recorded with mixing times of 120 and 100 ms, respectively, whereas the 3D ^{1}H-^{15}N HMQC-NOESY-HMQC spectrum was recorded with a mixing time of 150 ms. For the ^{15}N-separated NOESY spectrum, the spectral width and number of points acquired were 11.4 ppm and 128 complex points in ^{1}H(F_1), 30.01 ppm and 32 complex points in ^{15}N(F_2), and 13.44 ppm and 1024 real points in ^{1}H(F_3) with the ^{1}H and ^{15}N carrier frequencies placed at 4.67 and 115 ppm, respectively. For the ^{13}C-separated NOESY spectrum, the spectral width and numbers of points acquired were 9.26 ppm and 128 complex points in ^{1}H(F_1), 20.71 ppm and 32 complex points in ^{13}C(F_2), and 10.04 ppm and 512 real points in ^{1}H(F_3) with the ^{1}H and ^{13}C carrier frequencies placed at 4.3 and 63.71 ppm, respectively. Finally, for the ^{1}H-^{15}N HMQC-NOESY-HMQC spectrum, the spectral width in the ^{15}N(F_1 and F_2) dimensions was 30.01 ppm with the carrier at 115 ppm, and in the ^{1}H(F_3) dimension was 13.44 ppm with the carrier at 4.67 ppm, and 64 complex points were acquired in F_1, 32 complex points in F_2, and 1024 real points in F_3. All of the spectra were processed with a single zero filling in all dimensions on a Sun Sparc Workstation with in-house routines for Fourier transformation [L. E. Kay, D. Marion, A. Bax, *ibid.* **84**, 72 (1989)], together with the commercially available software package NMR2 (New Methods Research, Inc., Syracuse, New York). Analysis of the 3D spectra and peak picking was carried out with the in-house programs CAPP and PIPP [D. S. Garrett, R. Powers, A. M. Gronenborn, G. M. Clore, *ibid.* **95**, 214 (1991)].
8. Recombinant human IL-4 was expressed in yeast, uniformly isotopically labeled (with either ^{15}N or both ^{15}N and ^{13}C) and purified as described previously (*9, 30*). The version of IL-4 used includes the four-residue sequence Glu-Ala-Glu-Ala at the amino-terminus of the recombinant protein which is not part of the natural human IL-4. In this report residues are numbered from the amino-terminal Glu as residue 1, so that the natural IL-4 sequence starts at residue 5. In addition, the two potential N-linked glycosylation sites at Asn^{42} and Asn^{109} have been changed to Asp by site-directed mutagenesis to prevent hyperglycosylation in the yeast host (*29*).
9. R. Powers *et al.*, *Biochemistry* **31**, 4336 (1992); B. S. Garrett *et al.*, *ibid.*, p. 4347.
10. C. Redfield *et al.*, *ibid.* **30**, 11029 (1991).

11. G. M. Clore *et al.*, *EMBO J.* **5**, 2729 (1986).
12. Upper distance limits for distances involving methyl and methylene protons were corrected appropriately for center averaging [K. Wüthrich, M. Billetter, W. Braun, *J. Mol. Biol.* **169**, 949 (1983)]. In addition, 0.5 Å was added to the upper limits of distances involving methyl protons to account for the higher apparent intensity of methyl resonances [G. M. Clore, A. M. Gronenborn, M. Nilges, C. A. Ryan, *Biochemistry* **26**, 8012 (1987)].
13. The $^3J_{HN\alpha}$ coupling constants were obtained from an HMQC *J* spectrum [L. E. Kay and A. Bax, *J. Magn. Reson.* **86**, 110 (1990)] as described previously [J. D. Forman-Kay, A. M. Gronenborn, L. E. Kay, P. T. Wingfield, G. M. Clore, *Biochemistry* **29**, 1566 (1990)]. For $^3J_{HN\alpha} < 6$ Hz and > 8 Hz, ϕ was restrained to $-50 \pm 40°$ and $-125 \pm 50°$, respectively [A. Pardi, M. Billeter, K. Wüthrich, *J. Mol. Biol.* **180**, 741 (1984)].
14. Restraints on ψ of $-50 \pm 60°$ in the regions of regular helix, as delineated by NH(*i*)-NH(*i*+1), CαH(*i*)-NH(*i*+2,3,4] and CαH(*i*)-CβH(*i*+3) NOEs and the presence of slowly exchanging amide protons (*16*), were introduced on the basis of the $^{13}C\alpha$ and $^{13}C\beta$ chemical shifts [S. Spera and A. Bax, *J. Am. Chem. Soc.* **113**, 5490 (1991)].
15. Slowly exchanging NH protons were identified by recording a series ^1H-^{15}N Overbodenhausen correlation spectra [G. Bodenhausen and D. J. Ruben, *Chem. Phys. Lett.* **69**, 185 (1980); A. Bax, M. Ikura, L. E. Kay, D. A. Torchia, R. Tschudin, *J. Magn. Reson.* **86**, 304 (1990)] over a period of ~24 hours starting within 5 min of dissolving an unexchanged sample of lyophilized protein in D_2O.
16. K. Wüthrich, *NMR of Proteins and Nucleic Acids* (Wiley, New York, 1986).
17. G. M. Clore and A. M. Gronenborn, *Science* **252**, 1390 (1991).
18. The coordinates of the 22 SA structures and of the restrained minimized mean structure, (SA)r, together with the experimental restraints, have been deposited in the Brookhaven Protein Data Bank.
19. M. Nilges, G. M. Clore, A. M. Gronenborn, *FEBS Lett.* **229**, 317 (1988).
20. The hybrid distance geometry–SA protocol of (*19*) makes use of the program XPLOR [A. T. Brünger, G. M. Clore, A. M. Gronenborn, M. Karplus, *Proc. Natl. Acad. Sci. U.S.A.* **83**, 3810 (1986); A. T. Brünger, *XPLOR Version 3 Manual* (Yale University, New Haven, 1992)] incorporating a distance geometry module [J. Kusczewski, M. Nilges, A. T. Brünger, *J. Biomol. NMR* **2**, 33 (1992)]. The protocol involves first calculating an initial set of substructures incorporating only about one third of the atoms by projection from *n*-dimensional distance space into cartesian coordinate space, followed by SA with all atoms. The target function that is minimized during SA (as well as in conventional Powell minimization) comprises only quadratic harmonic potential terms for covalent geometry (that is, bonds, angles, planes, and chirality), square-well quadratic potentials for the experimental distance and torsion-angle restraints (*11*), and a quartic van der Waals repulsion term for the nonbonded contacts (*19*). All peptide bonds were restrained to be trans. There were no hydrogen-bonding, electrostatic, or 6-12 Lennard-Jones empirical potential energy terms in the target function.
21. B. R. Brooks *et al.*, *J. Comput. Chem.* **4**, 1987 (1983).
22. D. Eisenberg and A. D. McLachlan, *Nature* **319**, 199 (1986); L. Chiche, L. M. Gregoret, F. E. Cohen, P. A. Kollman, *Proc. Natl. Acad. Sci. U.S.A.* **87**, 3240 (1990).
23. In addition to deducing the approximate location of the main secondary structure elements from a qualitative analysis of the sequential and medium-range NOE data involving backbone protons, Redfield *et al.* (*10*) also presented six preliminary structures of IL-4 based on a very limited set of long-range NOE data. The precision of these structures, which had a backbone atomic rms difference of 3.2 Å (2.7 Å for the four helices), was only sufficient to suggest that the approximate topology probably comprised a left-handed four-helix bundle. Thus, the relative orientation of the four helices in their preliminary structures was very poorly defined and the packing of the four helices could not be defined at all. The difference in quality between these preliminary structures and those presented in this report does not therefore reflect a minor quantitative improvement in precision, but rather reflects a qualitative difference similar in nature, for example, to that between a 7 and 2.5 Å resolution x-ray structure.
24. S. S. Abdel-Meguid *et al.*, *Proc. Natl. Acad. Sci. U.S.A.* **84**, 6434 (1987).
25. A. M. de Vos, M. Ultsch, A. A. Kossiakoff, *Science* **255**, 306 (1992).
26. K. Diedrichs, S. Jacques, T. Boone, P. A. Karplus, *J. Mol. Biol.* **21**, 55 (1991); K. Diedrichs, T. Boone, P. A. Karplus, *Science* **254**, 1779 (1991).
27. D. Cosman *et al.*, *Trends Biochem. Sci.* **15**, 265 (1990); K. I. Arai *et al.*, *Annu. Rev. Biochem.* **59**, 7983 (1990); J. F. Bazan, *Proc. Natl. Acad. Sci. U.S.A.* **87**, 6934 (1990); S. Davies *et al.*, *Science* **253**, 59 (1991); D. P. Gearing *et al.*, *EMBO J.* **10**, 2839 (1991).
28. C. Carr, S. Aykent, N. M. Kimack, A. D. Levine, *Biochemistry* **30**, 1515 (1990).
29. B. M. Curtis *et al.*, *Proteins* **11**, 111 (1991).
30. L. S. Park, D. Friend, K. Grabstein, D. L. Urdal, *Proc. Natl. Acad. Sci. U.S.A.* **84**, 1669 (1987); L. S. Park, D. Friend, H. M. Sassenfeld, D. L. Urdal, *J. Exp. Med.* **166**, 476 (1987).
31. K. Grabstein *et al.*, *J. Exp. Med.* **163**, 1405 (1986); T. Yokota *et al.*, *Proc. Natl. Acad. Sci. U.S.A.* **83**, 5894 (1986).
32. M. Carson, *J. Mol. Graphics* **5**, 103 (1987).
33. Supported by the AIDS Directed Anti-Viral Program of the Office of the Director of the National Institutes of Health (G.M.C. and A.M.G.).

16 March 1992; accepted 23 April 1992

Rational Design of Potent Antagonists to the Human Growth Hormone Receptor

Germaine Fuh, Brian C. Cunningham, Rikiro Fukunaga, Shigekazu Nagata, David V. Goeddel, James A. Wells*

A hybrid receptor was constructed that contained the extracellular binding domain of the human growth hormone (hGH) receptor linked to the transmembrane and intracellular domains of the murine granulocyte colony-stimulating factor receptor. Addition of hGH to a myeloid leukemia cell line (FDC-P1) that expressed the hybrid receptor caused proliferation of these cells. The mechanism for signal transduction of the hybrid receptor required dimerization because monoclonal antibodies to the hGH receptor were agonists whereas their monovalent fragments were not. Receptor dimerization occurs sequentially—a receptor binds to site 1 on hGH, and then a second receptor molecule binds to site 2 on hGH. On the basis of this sequential mechanism, which may occur in many other cytokine receptors, inactive hGH analogs were designed that were potent antagonists to hGH-induced cell proliferation. Such antagonists could be useful for treating clinical conditions of hGH excess, such as acromegaly.

Knowledge of the molecular basis for hormone action is key to the rational design of hormone agonists and antagonists. High-resolution mutational analysis (*1*, *2*) and x-ray crystallographic studies (*3*) have defined two sites on hGH for binding two molecules of the extracellular domain of its receptor (hGHbp) (*4*). Dimerization of the hGHbp occurs sequentially, such that a hGHbp molecule binds to site 1 and then a second hGHbp molecule binds to both site 2 on hGH and a site on the first hGHbp (Fig. 1). A thorough examination of the biological importance of this model has been precluded because of the lack of an adequate cellular signaling assay for hGH. Here, we constructed a sensitive, cell-based assay for hGH, investigated the mechanism for signal transduction, and applied the assay for the design of antagonists to the hGH receptor.

The hGH receptor belongs to a large family of receptors of hematopoietic origin (*5*) that includes the interleukin-3 (IL-3) and granulocyte colony-stimulating factor (G-CSF) receptors. An IL-3–dependent myeloid leukemia cell line (FDC-P1) transfected with the full-length murine G-CSF (mG-CSF) receptor is stimulated to proliferate by G-CSF without IL-3 (*6*). We constructed a hybrid receptor that contained the hGHbp linked to a portion of the mG-CSF receptor containing the three extracellular fibronectin repeats and the transmembrane and intracellular domains (*7*). The fibronectin domains do not participate in the binding of G-CSF but are required for efficient expression of the mG-CSF receptor (*6*).

Competitive displacement of ^{125}I-labeled hGH from hybrid receptors on whole cells was used to establish the affinity for hGH and the approximate number of receptors per cell (*8*). In several independent

G. Fuh, B. C. Cunningham, J. A. Wells, Department of Protein Engineering, Genentech, Inc., 460 Point San Bruno Boulevard, South San Francisco, CA 94080.
R. Fukunaga and S. Nagata, Osaka Bioscience Institute, 6-2-4 Furuedai, Suita-shi, Osaka 565, Japan.
D. V. Goeddel, Department of Molecular Biology, Genentech, Inc., 460 Point San Bruno Boulevard, South San Francisco, CA 94080.

*To whom correspondence should be addressed.